Accepted for publication by Vehicle System Dynamics, 28 September 2019

Analysis of the Consistency of the Sperling Index for Rail Vehicles based on different Algorithms

Chenxin Deng[a] Jinsong Zhou[a] David Thompson[b] Dao Gong[a] Wenjing Sun[a] Yu Sun[a]

a. Institute of Railway Transit, Tongji University, Shanghai 201800, China;

b. Institute of Sound and Vibration Research, University of Southampton, University Road, Highfield, Southampton, SO17 1BJ, United Kingdom

Abstract: Ride comfort indices are used to evaluate the vibration of rail vehicles and to measure the discomfort of passengers. Among the various ride comfort indices, the Sperling index is widely used in China and other countries. However, there are several different methods for determining the Sperling index from dynamic simulations and performance measurements of rail vehicles, and the results obtained by different algorithms are inconsistent. It is therefore difficult to make an accurate evaluation with the different calculation results. In this paper, a comparison is made between algorithms based on time domain and frequency domain analysis and using the second and third powers of the acceleration. The different algorithms are then summarized into a unified equation, and the consistency of the results is analyzed by this equation. It is found that only the r.m.s-based algorithm in the time or frequency domain is stable when analysis is carried out over different sample times. The time-frequency consistency of the r.m.s-based algorithms is verified by Parseval's theorem and using calculation results from time domain simulations.
Key words: rail vehicle dynamics simulation; ride comfort index; Sperling index

1 Introduction

An important source of discomfort for railway passengers comes from the vibration of the vehicles. Vibration will not only cause fatigue of passengers, but in extreme cases may also cause internal organs and body to resonate with external vibration. It is also related to the ride quality and safety of rail vehicles [1]. Vibration of rail vehicles is extremely complicated, mainly because of the uncertainty in the vibration environment, including the vehicle suspension system, wheel profiles, design parameters of the vehicle body and the train speed [2]. When considering the impact of rail vehicle vibration on passengers, the weighted acceleration is generally used to quantify the severity of human exposure to the vibration environment [3], from which ride quality indices or ride comfort indices of rail vehicles can be calculated. These indices are an important aspect in the evaluation of the performance of rail vehicles. In the evaluation of the vibration level or ride comfort of rail vehicles, it is important that the calculation method provides consistent and reliable results.

To evaluate the ride quality or ride comfort of rail vehicles, it is necessary to consider the passengers' perception of the vibration, that is, to quantify human response by using appropriate weighting methods as part of the evaluation. The most commonly accepted principles of vibration perception assessment [4] are laid out in the international standard ISO 2631 [3, 5-7], the evaluation criteria based on the Sperling index [8-10], and the standard UIC 513 [11] proposed by the International Union of Railways and included in the European standard EN 12299 [12]. However, in different countries, the choice of general criteria are different due to the differences between rail vehicles, tracks and vibration environments. In some areas of Japan and South Korea [2], most passengers of the subways have to stand due to the crowding, so it is meaningless to evaluate the ride comfort for a sitting posture or allowing for seats. Indices from ISO 2631 and UIC 513 are based on vibration in three directions, while the Sperling index can be used to evaluate vertical or lateral vibration independently. In China, "Dynamic Vehicle Performance Evaluation and Test Identification Specification" [8] based on the Sperling index is widely used to study the dynamic characteristics of rail vehicles and evaluate the performance of rail vehicles, and is still in use today.

The Sperling index originated in the 1940s and 1950s [13]. To establish a baseline of ride comfort for rail vehicles, Helberg and Sperling conducted a test with 25 subjects by using a vibration test platform, and proposed the W_z (Werzungzahl) method to calculate ride quality indices by weighting the discrete spectrum and accumulating the third powers of the various frequency components. In a specified time interval, the Sperling index can also be calculated from the root mean square of the weighted acceleration in the frequency domain [14]. Kim [15] et al. determined the Sperling index by integrating the weighted power spectrum. Garg [16] showed that the Sperling index can be obtained by integrating the filtered acceleration in the time domain or frequency domain. Although there are different calculation formulae for determining the Sperling index, they are all widely used in the field of rail transport [17]. In addition to the calculation methods based on time-domain or frequency-domain data, Zhou [13] proposed a covariance method to calculate the weighted root mean square based on state space theory and determined the Sperling index directly. The indices in the ISO 2631 and UIC 513 methods are calculated using the second powers of the measured acceleration, i.e. based on the weighted root mean square value, whereas the Sperling index can be calculated by using either the second or third powers of the acceleration [16]. ISO 2631 does not specify a sampling time. When calculating the index by UIC 513, the 95th percentile values of 60 separate 5-sec measurements are taken for each direction and the index is evaluated as six times the root sum of squares of these values. In the Chinese standard GB 5599-85 [8], the sampling time used for determining the Sperling index should be selected between 18 s and 20 s, but in practice, in performance measurements at certain speeds, it is difficult to maintain the specified sampling time length. The calculation results of the Sperling index are inconsistent because of the different algorithms, sample time length and frequency sample interval, which makes it difficult to evaluate ride quality accurately. Nevertheless, the inconsistency of the Sperling index has not attracted the attention of researchers in the field of rail transit.

In this paper, the dependence of the Sperling index on the algorithm used and the sampling time is investigated using dynamic simulations and performance measurements of rail vehicles. In order to analyze the consistency of the Sperling index, the frequency-domain calculation methods are summarized into a unified formula, which is used to identify a stable frequency-domain calculation method. Based on Parseval's theorem [12], the time-frequency consistency and the stability of the Sperling index based on root mean square is demonstrated by the time-domain data in dynamics simulation.

2 Calculation of Sperling index for rail vehicles

2.1 General method of Sperling index

Garg [16] showed that, if the vibration acceleration spectrum of the vehicle body is a continuous function of frequency, a weighting function can be used to weight the time-domain or frequency-domain acceleration sequence. Then, the Sperling index can be calculated from the weighted acceleration by the following alternative equations, based on the cube of the acceleration:

$$W_{3F} = \left(\int_0^{Fs} A_B(f)^3 df \right)^{1/10} \tag{1}$$

$$W_{3T} = \left(\frac{1}{T} \int_t^{t+T} \left| a_B(t) \right|^3 dt \right)^{1/10} \tag{2}$$

or based on the squared acceleration:

$$W_{2F} = \left(\int_0^{Fs} A_B(f)^2 df \right)^{1/6.67} \tag{3}$$

$$W_{2T} = \left(\frac{1}{T} \int_t^{t+T} a_B(t)^2 dt \right)^{1/6.67} \tag{4}$$

where $A_B(f)$ represents a continuous weighted acceleration spectrum as a function of frequency, and $a_B(t)$ represents

a continuous weighted acceleration time history; F_s represents the maximum analysis frequency and T is the analysis time.

2.2 Sperling index calculated using measured data

Ride comfort tests are required during the service of rail vehicles. At the request of a rail vehicle operating company, a ride comfort test of a rail vehicle with a running distance of about 100,000 km has been carried out. When arranging the measuring points, the acceleration sensor was fixed on a steel plate, and the steel plate was placed at the center and the end of the vehicle body under test. Each measuring point includes three channels, of which the horizontal and vertical directions are used here, the sampling frequency is 512 Hz, and the test speed is 200 km/h. Fig. 1 and Fig. 2 show the placement of the measurement points and the analysis equipment, respectively. Fig. 3 shows part of the vibration acceleration data from the center of the vehicle body.

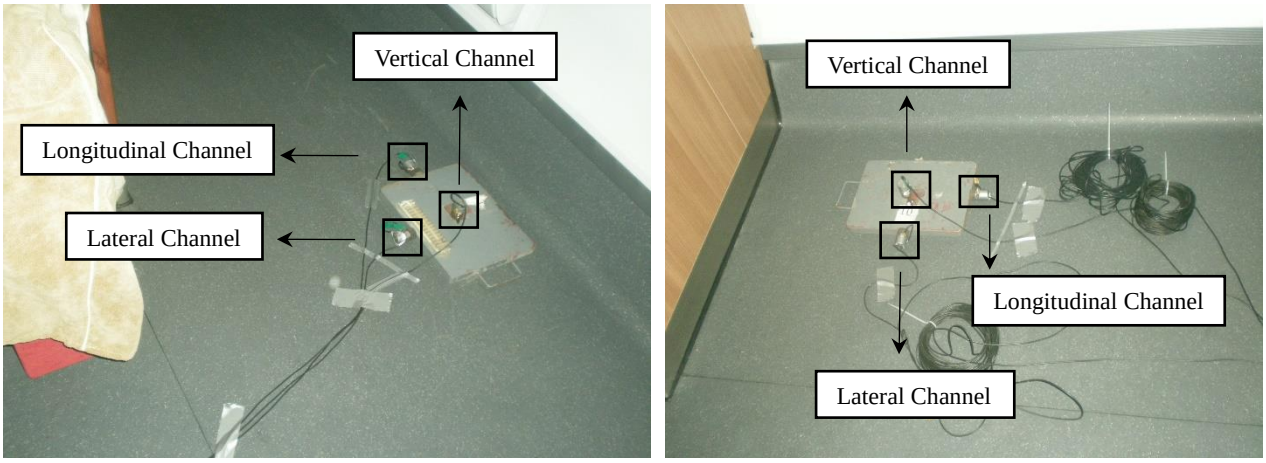

Fig.1 Schematic diagram of measuring points

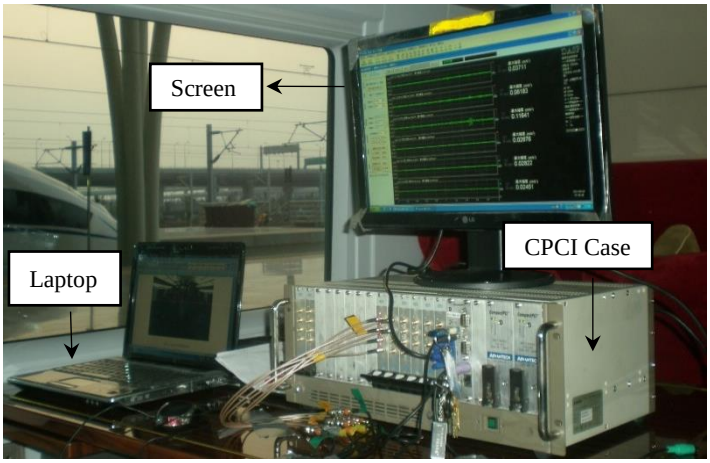

Fig.2 Data acquisition and analysis equipment

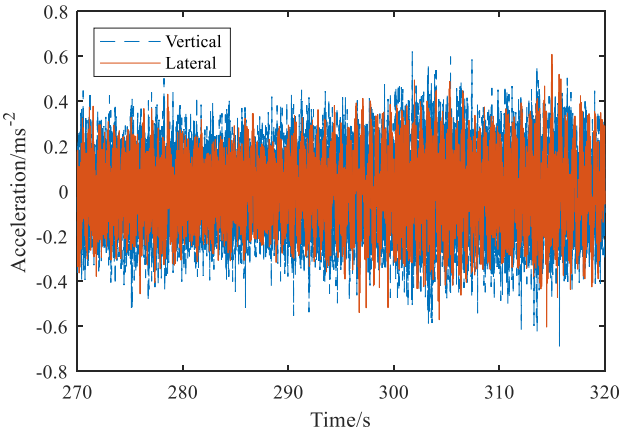

Fig.3 Vibration acceleration data from the center of vehicle body at 200 km/h

The vertical and lateral Sperling indices have been calculated based on the different formulae (1-4) from the measurement data. These can be rated according to Tab. 1.

Tab.1 Perception of ride comfort index *W*

Vibration level	Ride quality	Ride comfort index
Just noticeable	Very good	<1.0
Clearly noticeable	Good	1.0~2.0
Pronounced but not unpleasant		2.0~2.5
Strong but tolerable	Tolerable	2.5~3.0
Very strong and unpleasant		3.0~3.5
Extremely strong and unpleasant	Not tolerable	3.5~4.0

In the process of actual measurement, it was found that the sampling time length has a great effect on the calculation results of the Sperling index. This is illustrated with results for the vertical direction. When the test train ran for different sample times at the same speed on the same track segment, the calculated results of Sperling index are different. Tab. 2 shows the calculated vertical Sperling index obtained from different sampling times using the measured acceleration.

Tab.2 Calculation result from different sample time and formulae

T (s)	W_{3F}	W_{3T}	W_{2F}	W_{2T}
10	1.839	1.799	2.167	2.149
20	1.776	1.721	2.165	2.152
50	1.696	1.634	2.166	2.149
100	1.639	1.597	2.166	2.150
200	1.583	1.536	2.166	2.150

To obtain these results, the whole sampled dataset was divided into segments of length *T* seconds, which is called the sample time length here. When calculating the Sperling index, index values are calculated for separate segments of length *T* seconds and the Sperling index is evaluated as the mean of these values. The Sperling index estimates W_{2F} and W_{2T} calculated by Equations (3, 4) are both more than 2 (pronounced but not unpleasant) and do not change with the sample time, whereas the estimates W_{3F} and W_{3T} calculated by Equations (1, 2) are less than 2 and the results decrease as the sample time *T* is increased. For a sample length of 20 s, as required by [8], these formulae give a result around 1.7 compared with 2.2 from Equations (3, 4), a difference of around 20%. Such deviations are clearly inconsistent with the actual response of the occupants and lead to different ratings according to Tab. 1. Since the calculation results are not uniform, it is difficult to make a consistent evaluation of ride comfort of this test vehicle.

2.3 Sperling index calculated using simulation data

In addition to this measured data, the various formulae are assessed using simulated data from a 23-degree-of-freedom rail vehicle model. The equations of motion for this model are presented in the appendix. It includes the lateral displacement and the yaw displacement of four wheelsets, and the lateral, vertical, roll, pitch and yaw displacements of two bogie frames and the car body. A schematic diagram of the model is shown in Fig. 4.

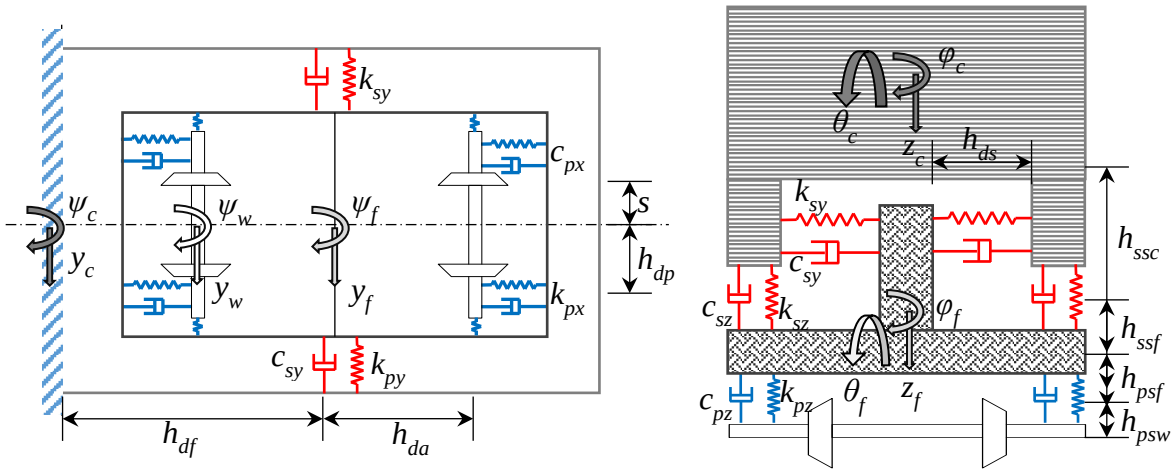

Fig.4 Schematic diagram of vehicle model

The general matrix equations of motion for this 23-degree-of-freedom system can be written as,

$$\boldsymbol{M}\ddot{\boldsymbol{Z}} + \boldsymbol{C}\dot{\boldsymbol{Z}} + \boldsymbol{K}\boldsymbol{Z} = \boldsymbol{D}_w\boldsymbol{Z}_w \tag{5}$$

where, $\boldsymbol{Z}_w = (y_{w1}, y_{w2}, y_{w3}, y_{w4}, z_{w1}, z_{w2}, z_{w3}, z_{w4}, \dot{z}_{w1}, \dot{z}_{w2}, \dot{z}_{w3}, \dot{z}_{w4})^T$, $\boldsymbol{Z} = (y_{w1}, \psi_{w1}, y_{w2}, \psi_{w2}, y_{w3}, \psi_{w3}, y_{w4}, \psi_{w4}, y_{f1}, z_{f1}, \varphi_{f1}, \theta_{f1}, \psi_{f1}, y_{f2}, z_{f2}, \varphi_{f2}, \theta_{f2}, \psi_{f2}, y_c, z_c, \varphi_c, \theta_c, \psi_c)^T$.

It is assumed that the track irregularity input to each wheelset can be derived from that of the first wheelset with a simple delay. The inputs of the various wheelsets are therefore completely correlated, and the virtual excitation method [13] can be used to simulate the vehicle dynamic response in the frequency domain. According to Eq. (5), the power spectrum analysis method based on the virtual excitation method is proposed. The time histories of the irregularity input of each wheelset are contained in the vector $\boldsymbol{f}(t)$.

$$\boldsymbol{f}(t) = \left(f(t-\tau_1) \quad f(t-\tau_2) \quad \ldots \quad f(t-\tau_r) \right)^T \tag{6}$$

where τ_r is the delay of the r-th wheelset relative to the first one. The power spectral density function of $f(t)$ is $S_f(\omega)$, and its virtual excitation can be written as,

$$\tilde{\boldsymbol{f}}(t) = \left(e^{-i\omega\tau_1} \quad e^{-i\omega\tau_2} \quad \ldots \quad e^{-i\omega\tau_r} \right)^T \sqrt{S_f(\omega)} e^{i\omega t} \tag{7}$$

Substituting Eq. (7) into Eq. (5) yields,

$$\boldsymbol{M}\ddot{\tilde{\boldsymbol{Z}}} + \boldsymbol{C}\dot{\tilde{\boldsymbol{Z}}} + \boldsymbol{K}\tilde{\boldsymbol{Z}} = \boldsymbol{D}_w\tilde{\boldsymbol{f}}(t) \tag{8}$$

The response of the system is then obtained as,

$$\tilde{\boldsymbol{Z}} = \left(-\boldsymbol{M}\omega^2 + \boldsymbol{C}i\omega + \boldsymbol{K} \right)^{-1} \boldsymbol{D}_w \left(e^{-i\omega\tau_1} \quad e^{-i\omega\tau_2} \quad \ldots \quad e^{-i\omega\tau_r} \right)^T \sqrt{S_f(\omega)} e^{i\omega t} \tag{9}$$

Therefore, the power spectral density matrix for each degree of freedom can be calculated as,

$$\boldsymbol{S}_z = \tilde{\boldsymbol{Z}}^* \cdot \tilde{\boldsymbol{Z}}^T \tag{10}$$

where * and ^{T} represent conjugation and transposition, respectively.

The vehicle parameters used are listed in the Appendix. In the simulations, the German high-speed spectrum

[13] is selected as the input of the track irregularity, as shown in Fig. 5(a). The spectra of vertical acceleration response of the vehicle body and bogie frame are obtained from the response matrix $\boldsymbol{S}_z$ by converting the corresponding displacements to accelerations and these are shown in Fig. 5(b) for a train speed of 200 km/h.

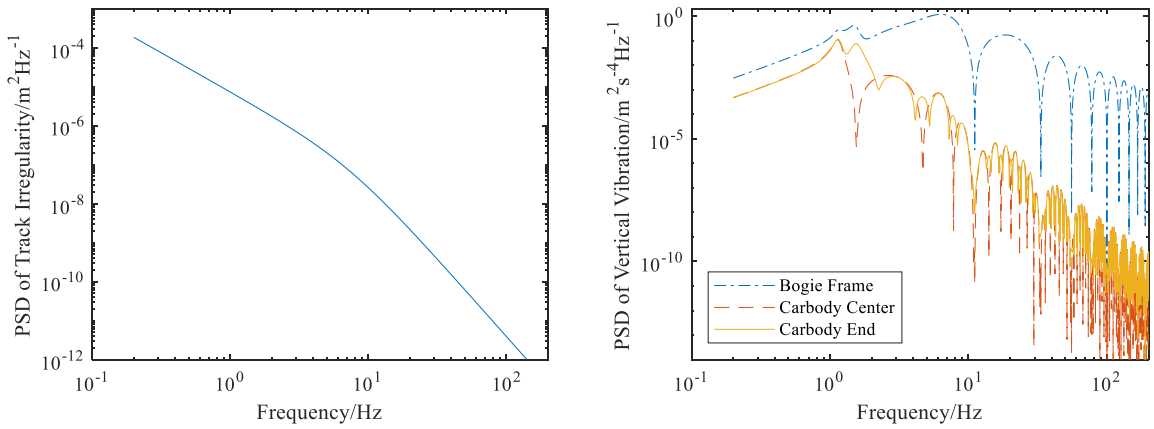

(a) (b)

Fig.5 (a) Assumed PSD of track irregularities; (b) PSD of vertical acceleration of bogie frame, carbody center and carbody end for speed 200 km/h

The weighted power spectral density of the acceleration, denoted as $S_B(f)$, can be calculated by applying the appropriate weighting function to the spectra in Fig. 5. The weighted amplitude of the acceleration $A_B(k)$ at a certain frequency f_k can be obtained from

$$A_B(k)^2 = S_B(f_k)\Delta f \tag{11}$$

where Δf represents the sampling interval in the frequency domain. Thence, the Sperling index W_z can be calculated from Eqs. (1, 3).

Simulations are performed for running speeds between 150 and 350 km/h. The effective excitation frequency range of the spectrum is selected as 0.1 Hz to 500 Hz with a sampling interval of 0.05 Hz (this corresponds to a sample length of 20 s). Fig. 6 shows the variation of the Sperling index with train speed according to Eqs. (1, 3). When the speed is 200 km/h, the results calculated according to Eqs. (1, 3) are W_{3F} = 1.719 and W_{2F} = 2.014 respectively, which differ by 17.1%.

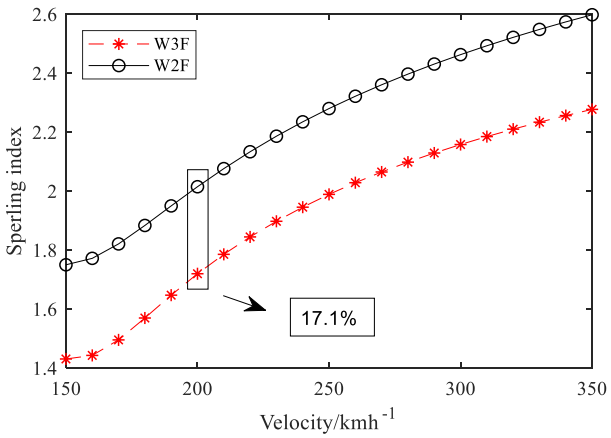

Fig.6 Sperling indices obtained in the frequency domain W_{2F} and W_{3F} from simulations for different train speeds

Next, using Eq. (1), different sampling intervals in the frequency domain $\Delta f = 1/T$ are selected, and the corresponding variation of Sperling index W_{3F} with speed is calculated. Fig. 7 shows results for sampling intervals

of 0.005 Hz, 0.01 Hz, 0.02 Hz, 0.05 Hz, and 0.1 Hz, corresponding to time intervals of 200, 100, 50, 20 and 10 s respectively. From Fig. 7, at a given speed, as the sampling interval in the frequency domain decreases, the Sperling index W_{3F} decreases. For example, for a speed of 200 km/h the Sperling index W_{3F} result differs by 16.5% between a sampling interval in the frequency domain of 0.005 Hz and 0.1 Hz. The results for W_{2F} (not shown) do not vary with sampling interval.

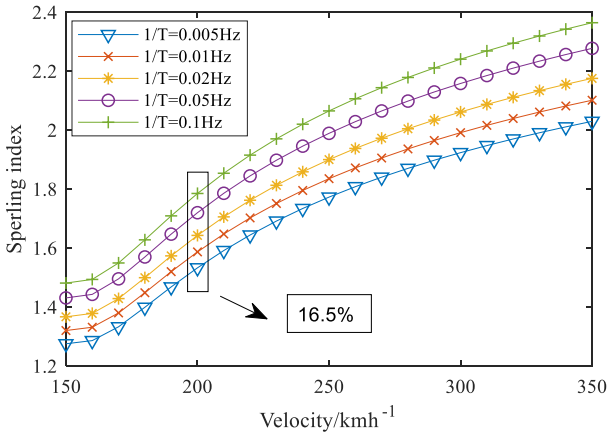

Fig.7 Sperling index W_{3F} from simulations with different frequency intervals

When calculating the Sperling index from simulations, different calculation formulae and sampling intervals in the frequency domain lead to differences in the calculation results. Since the calculation results are not uniform, it is difficult to give a consistent evaluation of the ride comfort of this simulated vehicle. In the process of measurement and simulation, the inconsistency of the Sperling index has a great influence on the evaluation of the performance of rail vehicles. Therefore, it is necessary to analyze the different calculation methods for the Sperling index to determine the source of the inconsistency.

3 Analysis of the algorithm of Sperling index

3.1 Principle of calculation method

According to the W_z method proposed by Sperling [10], the original calculation equation of ride comfort index [8] is written as follows.

$$W_z = 0.896\left(\frac{A^3}{f}F(f)\right)^{1/10} \tag{12}$$

where W_z represents the Sperling index; A is the acceleration amplitude, with units m/s^2; f is the oscillation frequency, with units Hz; $F(f)$ is a frequency-dependent factor that expresses human vibration sensitivity [8]. Accelerations measured on the car body do not have a single frequency but a whole spectrum, so the measured data is usually decomposed into N segments in the frequency domain, the amplitude of the acceleration of each segment frequency is obtained, and the value W_{zk} of each segment can be calculated. Therefore, the total Sperling index can be obtained from

$$W = \left(\sum_{k=0}^{N-1} W_{zk}^{10}\right)^{1/10} = \left(\sum_{k=0}^{N-1}\left(A(k)\cdot\left(0.896^{10}F(f_k)/f_k\right)\right)^3\right)^{1/10} = \left(\sum_{k=0}^{N-1} A_B(k)^3\right)^{1/10} \tag{13}$$

where $A_B(k)$ represents the weighted amplitude of acceleration at a certain frequency f_k.

Since the simulated and measured signals are both discrete, the corresponding spectrum is also discrete. Therefore, the integrals Eqs. (1, 3) in the frequency domain can be discretized as,

$$W_{3F} = \left(\int_0^{Fs} A_B(f)^3 df \right)^{1/10} = \left(\sum_{k=0}^{N-1} A_B(k)^3 \right)^{1/10} \tag{14}$$

$$W_{2F} = \left(\int_0^{Fs} A_B(f)^2 df \right)^{1/6.67} = \left(\sum_{k=0}^{N-1} A_B(k)^2 \right)^{0.15} \tag{15}$$

and these can be written in general form as,

$$W_{mF} = \left(\sum_{k=0}^{N-1} A_B(k)^m \right)^{0.3/m} \tag{16}$$

When m is equal to 2, Eq. (16) is consistent with the calculation method mentioned in references [13-16], i.e. Eqs. (3, 4, 15); when m is equal to 3, Eq. (16) is consistent with the calculation method mentioned in references [8-10, 13, 16], i.e. Eqs. (1, 2, 13, 14). Eq. (16) thus unifies all calculation methods of the Sperling index in the frequency domain, which is convenient for subsequent analysis.

3.2 Consistency analysis with frequency spectrum

For a certain signal, the weighted spectrum $A_B(k)$ is deterministic and non-negative (see Eq. (11)). Therefore, W_m decreases as m increases because of the nature of the norm [18]:

$$\sum_{k=0}^{N-1} A_B(k) \geq \left(\sum_{k=0}^{N-1} A_B(k)^2 \right)^{1/2} \geq \left(\sum_{k=0}^{N-1} A_B(k)^3 \right)^{1/3} \geq \ldots \geq \left(\sum_{k=0}^{N-1} A_B(k)^m \right)^{1/m} \geq \ldots \geq \max A_B(k) \tag{17}$$

As seen already in the calculation results of the Sperling index obtained from measurements and simulations, Eq. (16) indicates that for signals with the same sampling frequency, and therefore the same sampling time length T, the index m will affect the calculation result of the Sperling index. Since the signal is discrete, the sample time length T can be adjusted by changing the number of sampling points N.

The acceleration signal of the vehicle body vertical vibration is obtained from the simulation model for different values of m. Fig. 8 shows the calculation results of the Sperling index obtained with different parameters. Different line types in the figure represent different sample time lengths. For a given sample time length, the calculation result reduces as the index m is increased, which is consistent with Eq. (17). If sample time length is 20 seconds, the calculation results for m = 2 or 3 are approximately 20% different. If m is greater than 2, the calculation result for the Sperling index decreases as the sample time length increases but if m is equal to 2, the Sperling index does not change with the sample time length. In this case the Sperling index can be calculated from the weighted r.m.s. acceleration of the vehicle body. Thus, the selection of the index m and the sample length T has a significant influence on the grading of the ride comfort in dynamic simulations and performance measurements of rail vehicles.

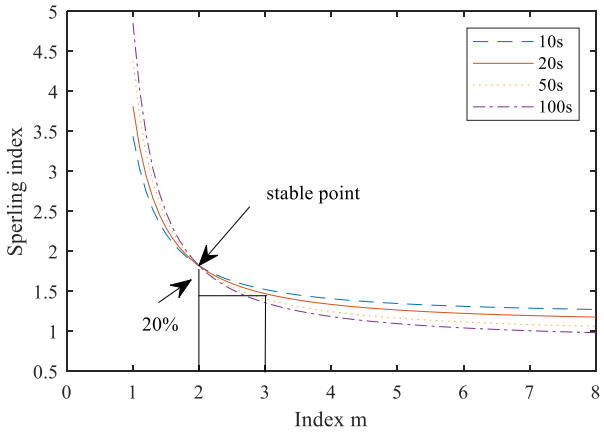

Fig.8 Sperling index W_{mF} changes with m for different sample times T

3.3 Consistency analysis with power spectral density

The virtual excitation method can be used to calculate the power spectral density matrix of acceleration responses from the simulation, allowing the weighted acceleration PSD of the vehicle body vertical vibration to be calculated as $S_B(f)$. The weighted vibration amplitude $A_B(k)$ at a certain frequency f_k can be calculated from Eq. (11) and substituted into Eq. (16) as follows,

$$W_{mF} = \left(\sum_{k=0}^{N-1} A_B(k)^m \right)^{0.3/m} = \left(\sum_{k=0}^{N-1} \left(\sqrt{S_B(f_k)\Delta f} \right)^m \right)^{0.3/m} = \Delta f^{\frac{3(m-2)}{20m}} \left(\sum_{k=0}^{N-1} \left(\sqrt{S_B(f_k)} \right)^m \cdot \Delta f \right)^{0.3/m} \tag{18}$$

If Δf satisfies a certain precision requirement, the summation part in Eq. (18) can be replaced by an integral result denoted as w_m,

$$W_{mF} = \Delta f^{\frac{3(m-2)}{20m}} \left(\int_0^{F_s} \left(\sqrt{S_B(f_k)} \right)^m df \right)^{0.3/m} = \Delta f^{\frac{3(m-2)}{20m}} \cdot w_m \tag{19}$$

For a given value of m, the integral result w_m is independent of Δf. When m is equal to 2, the integral result is denoted as w_2,

$$W_{2F} = \left(\int_0^{F_s} \left(\sqrt{S_B(f_k)} \right)^2 df \right)^{0.3/2} = w_2 \tag{20}$$

The Sperling index W_{2F} calculated by Eq. (20) does not change with Δf, that is, the result does not vary with sample time length T, which is consistent with the results shown in Fig. 8. However, when m is equal to 3, Eq. (19) is written as,

$$W_{3F} = \Delta f^{1/20} \left(\int_0^{F_s} \left(\sqrt{S_B(f_k)} \right)^3 df \right)^{0.3/3} = \Delta f^{1/20} \cdot w_3 \tag{21}$$

from which it can be seen that the result of W_{3F} decreases as Δf decreases.

Fig. 9 compares the variation of Sperling index W_{mF} with the frequency-domain sample interval Δf for the cases of m equal to 2 and 3; these results are obtained from the simulation model. It can be seen from Fig. 9 that the Sperling index W_{3F} calculated from Eq. (21) decreases with the decrease of frequency-domain sample interval Δf and it reduces according to $\Delta f^{1/20}$. Conversely, the Sperling index W_{2F} calculated from Eq. (20) is independent of the frequency-domain sample interval Δf, corresponding to the stable point in Fig. 8.

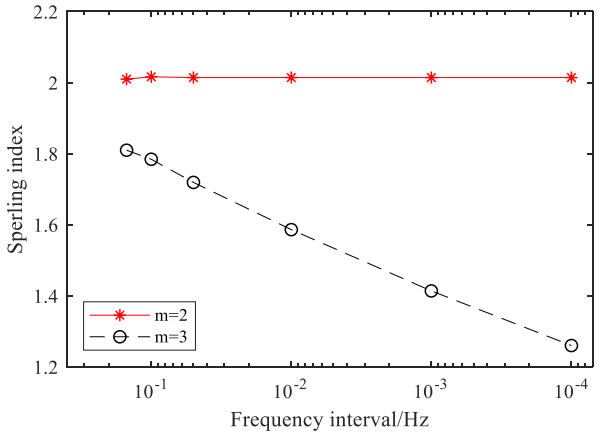

Fig.9 Sperling index W_{mF} based on simulations for different values of the index m and the frequency interval

Tab. 3 shows the calculation results from different frequency-domain sample intervals, where Δf is the frequency-domain sample interval, W_{2F} and W_{3F} are the Sperling index results with m equal to 2 and 3, and w_3 is the integral result in Eq. (19) with m equal to 3. When the frequency-domain sample interval is larger than 0.05 Hz, the r.m.s. of the vehicle body acceleration shows variations because the PSD is distorted by the large frequency-domain sample intervals in the simulations. However, when the frequency-domain sample interval is less than 0.05 Hz, the r.m.s. acceleration, Sperling index W_{2F} and the integral part w_3 all give stable results, whereas the unstable variation of the Sperling index W_{3F} is caused by the factor $\Delta f^{1/20}$. When the frequency-domain sample interval is 0.05 Hz, that is, the corresponding time-domain sample time length is 20 s, the Sperling index results W_{2F} and W_{3F} are 2.01 and 1.72, respectively, which differ by 15%. Therefore, the selection of the index m and the frequency-domain sample interval Δf has a significant effect on the calculation result in the process of simulation for ride comfort calculation.

It can be observed that, although they are not identical, w_2 and w_3 give similar values. The main difference between W_{3F} and W_{2F} comes from the factor $\Delta f^{1/20}$, which is equal to 1.16 (i.e. 16% difference) for Δf = 0.05 Hz (T = 20 s).

Tab.3 Calculation results from different methods in the frequency domain with different frequency intervals

Δf (Hz)	RMS (m/s^2)	W_{2F}	W_{3F}	w_3	$\Delta f^{1/20}$
0.20	0.180	1.983	1.787	1.937	0.923
0.15	0.189	2.010	1.810	1.990	0.910
0.10	0.191	2.016	1.775	1.992	0.891
0.05	0.190	2.014	1.719	1.997	0.861
10^{-2}	0.190	2.014	1.586	1.997	0.794
10^{-4}	0.190	2.014	1.260	1.997	0.631

On the basis of the above analysis, the different algorithms can be summarized into Eq. (16, 19). In the process of measurement and simulation of rail vehicles, different calculation results can be obtained from different formula parameters. The result is only stable when m is equal to 2, that is, the algorithm is based on the r.m.s. If the corresponding algorithm in the time domain can be derived according to this stable algorithm based on the r.m.s., the calculation process with time domain data can be used reliably, which is more rapid and straightforward.

4 Time-frequency transformation of Sperling index

4.1 Derivation of time-domain algorithm

In the process of measurement, a stable algorithm for the Sperling index in the time domain can be more rapid and simple to obtain without the need to apply Fourier transformation. Moreover, this would be consistent with the calculation of ride comfort indices according to the standards ISO 2631 and UIC 513 which are done in the time

domain. Based on the above analysis, the existence of a stable algorithm in the time domain will be established in this section. Among the equations given by Garg, Eqs. (1, 2) correspond to the third power, and Eqs. (3, 4) to the second power. However, the consistency between time and frequency domain indices has not been proven by Garg.

For a finite discrete signal $a(n)$, if the discrete Fourier transform is $X(k)$, and the number of sample points is N, then the spectrum $A(k)$ is,

$$A(k)=\frac{1}{N}\left|X(k)\right| \tag{22}$$

According to Parseval's theorem [13],

$$\begin{aligned}\sum_{n=0}^{N-1}\left|a(n)\right|^2&=\sum_{n=0}^{N-1}a(n)\cdot a(n)^*=\sum_{n=0}^{N-1}\left(\frac{1}{N}\sum_{k=0}^{N-1}X(k)e^{-\frac{i2\pi n}{N}k}\right)\cdot a(n)^*=\frac{1}{N}\sum_{k=0}^{N-1}\left(X(k)\sum_{n=0}^{N-1}\left(a(n)^*e^{-\frac{i2\pi k}{N}n}\right)\right)\\&=\frac{1}{N}\sum_{k=0}^{N-1}\left(X(k)\cdot X(k)^*\right)=\frac{1}{N}\sum_{k=0}^{N-1}\left|X(k)\right|^2=N\sum_{k=0}^{N-1}\left|A(k)\right|^2\end{aligned} \tag{23}$$

Therefore,

$$\frac{1}{N}\sum_{n=0}^{N-1}\left|a(n)\right|^2=\sum_{k=0}^{N-1}\left|A(k)\right|^2 \tag{24}$$

In order to convert the calculation process of the Sperling index from the frequency domain to the time domain, the weighting method needs to be expressed in the time domain, that is, the amplitude weighting in the frequency domain needs to be expressed as a filter in the time domain. Taking vertical vibration as an example, the weighting function [16] $B(f)$ is written as,

$$B(f)=0.59\left(\frac{1.9f^2+\left(0.25f^2\right)^2}{\left(1-0.28f^2\right)^2+\left(1.6f-0.04f^3\right)^2}\right)^{1/2} \tag{25}$$

and the transfer function $G(s)$ of the corresponding filter is written as,

$$G(s)=\frac{0.59\left(0.0063s^2+0.2200s\right)}{1.4836\times10^{-4}s^3+0.0070s^2+0.2488s+1} \tag{26}$$

Fig. 10 shows a comparison of the amplitude-frequency characteristics of the weighting function in Eq. (25) and the transfer function of the filter from Eq. (26), which can be seen to be identical.

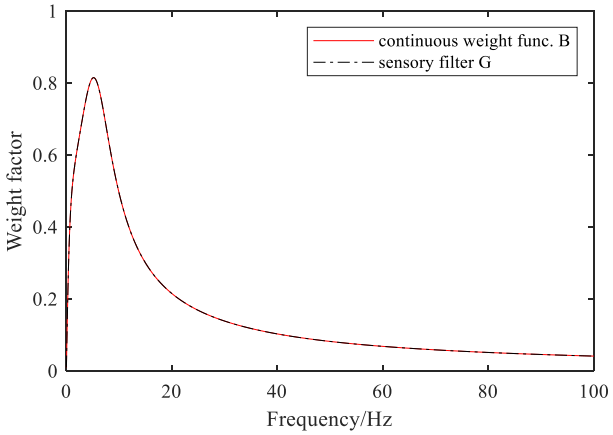

Fig.10 Amplitude-frequency characteristics of the filter for vertical vibration

With the equivalent weighting of time-domain and frequency-domain data, Eq. (24) can be written as,

$$\frac{1}{N}\sum_{n=0}^{N-1}\left|a_B(n)\right|^2=\sum_{k=0}^{N-1}\left|A_B(k)\right|^2 \tag{27}$$

Therefore, the calculation of Sperling index can be converted from frequency domain to time domain only if m is

equal to 2,

$$W_2 = \left(\sqrt{\sum_{k=0}^{N-1} \left(A_B(k) \right)^2} \right)^{0.3} = \left(\sqrt{\frac{1}{N} \sum_{k=0}^{N-1} \left(a_B(n) \right)^2} \right)^{0.3} = \left(\mathrm{RMS}_B \right)^{0.3} \tag{28}$$

where, $A_B(k)$, $a_B(n)$ and RMS_B represent the weighted frequency-domain sequence, the time-domain sequence and corresponding r.m.s. respectively. According to Eq. (28), the Sperling index can be directly calculated in the time domain and is related to the r.m.s. of filtered time-domain sequence. However, for the third power of acceleration, Eq. (2) cannot be derived from Eq. (1) by time-frequency conversion, and its time-frequency consistency cannot be proven. It may be noted from Tab. 2 that the results for W_{3F} and W_{3T} differ from one another by around 3%.

4.2 Verification of time-frequency consistency

By converting Eq. (5) to the state space equation, a time-domain simulation for the rail vehicle dynamic system is carried out.

$$\dot{\boldsymbol{X}} = \boldsymbol{A}\boldsymbol{X} + \boldsymbol{B}\boldsymbol{Z}_w \tag{29}$$

where, $\boldsymbol{X} = \begin{pmatrix} \boldsymbol{Z} \\ \dot{\boldsymbol{Z}} \end{pmatrix}$, $\boldsymbol{A} = \begin{pmatrix} \boldsymbol{0} & \boldsymbol{E} \\ -\boldsymbol{M}^{-1}\boldsymbol{K} & -\boldsymbol{M}^{-1}\boldsymbol{C} \end{pmatrix}$, $\boldsymbol{B} = \begin{pmatrix} \boldsymbol{0} \\ \boldsymbol{M}^{-1}\boldsymbol{D}_w \end{pmatrix}$.

In a simulation for a train speed of 200 km/h, the time-domain data of vertical acceleration of vehicle body has been obtained for the Sperling index calculation. Tab. 4 shows the calculation results from the time-domain and frequency-domain algorithm based on the r.m.s. with different sample time lengths, where W_{2F} and W_{2T} represent the results of the frequency-domain algorithm and time-domain algorithm with m equal to 2. Here, the results for W_{2F} are obtained from the time-domain simulations by applying an FFT to the results. The values of W_{2F} and W_{2T} do not change with the sample time length and differ only by 1.6% because of energy leakage when filtering with the digital filter. The algorithm of the Sperling index based on the r.m.s. is stable and its time-frequency consistency is demonstrated with the time-domain simulation data. Therefore, in the process of performance tests for the rail vehicle, it is recommended that this simple and stable time-domain algorithm based on filtered r.m.s. data should be selected for calculation of the Sperling index.

Tab.4 Calculation results from time-domain simulations

T (s)	RMS (m/s^2)	W_{2F}	W_{2T}
10	0.188	2.008	1.976
20	0.189	2.009	1.978
30	0.189	2.010	1.978
40	0.189	2.010	1.978
50	0.189	2.010	1.978

5 Conclusions

In this paper, the Sperling index calculated using different algorithms is shown to give inconsistent results in dynamic simulations and performance measurements of rail vehicles. The main conclusions are as follows:

1. Calculating the Sperling index in the frequency domain, different algorithms can be summarized into a unified formula. If the parameter m, representing the power of the weighted acceleration, is greater than 2, the calculation result of the Sperling index decreases as the sample time length in the time domain increases or the sample interval in the frequency domain decreases. Only if the parameter m is equal to 2, that is, the algorithm is based on r.m.s. values, is the Sperling index result stable with varying sample length.

2. When comparing results between those obtained from the formulae based on the second and third powers of acceleration, the Sperling index result based on the third power is around 15-20% smaller than that based on the second power when a 20 s sample time is used.

3. With the stable frequency-domain algorithm based on the r.m.s. values, a time-domain algorithm is derived based on Parseval's theorem. Its time-frequency consistency is also verified with the time-domain data from dynamic simulations of a rail vehicle. However, the time-frequency consistency of the algorithm with m equal to 3 cannot be proved and the results from time-domain and frequency-domain analysis are found to differ by around 3%. Therefore, it is recommended that the algorithm based on the r.m.s. in the time domain should be selected for rail vehicle measurements.

4. With the stable and time-frequency consistent algorithm based on the r.m.s., an accurate evaluation based on the Sperling index can be made in dynamic simulations and performance measurements of rail vehicles. The research in this paper can guide the calculation of ride comfort index and improve the dynamic performance evaluation system of rail vehicles.

References

[1] Zhou J, R Goodall, L Ren, et al. Influences of car body vertical flexibility on ride quality of passenger railway vehicles. Proceeding of the institution of mechanical engineers, Part F: Journal of Rail and Rapid Transit. 2009, 223(5): 461-471.

[2] Suzuki, H. Research trends on riding comfort evaluation in Japan. Proceedings of the Institution of Mechanical Engineers Part F Journal of Rail and Rapid Transit. 1998; 212(1), 61-72.

[3] ISO 2631-4. Mechanical Vibration and Shock-Evaluation of Human Exposure to Whole-Body Vibration. Part 4: Guidelines.

[4] Iwnicki, S. Handbook of Railway Vehicle Dynamics. 2006.

[5] ISO 2631 Guide for the evaluation of human exposure to whole-body vibration. 1978.

[6] ISO 2631-1 Evaluation of human exposure to whole-body vibration –Part I: General requirements. 1985.

[7] ISO 2631-1 Evaluation of human exposure to whole-body vibration – Part I: General requirements. 1997.

[8] GB 5599-85. Railway Vehicles-Specification for Evaluation the Dynamic Performance and Accreditation Test.

[9] Sperling E. Verfahren zur Beurteilung der Laufeigenschafen von Eisenbahnwesen. Organ Fortschritte des Eisenbahnwesens. 1941; 12, 176-187.

[10] Sperling E, Betzhold C. Beitrag zur Beurteilung des Fahrkomforts in Scheinenfahrzeugen. Glasers Annalen. 1956; 80, 314-320.

[11] UIC 513R. Guidelines for Evaluating Passenger Comfort in Relation to Vibration in Railway Vehicles.

[12] CEN, Railway Applications – Ride Comfort of Passengers – Measurement and Evaluation, prENV 12299. 1996.

[13] Zhou J S. Vibration and Control in Railway Vehicles. Beijing: China Railway Publishing House. 2012.

[14] Khan, M S, Sundstrom J. Effects of vibration on sedentary activities in passenger trains. Journal of Low Frequency Noise Vibration and Active Control. 2007; 26(1), 43-55.

[15] Kim YG, Kwon HB, Kim SW, et al. Correlation of ride comfort evaluation methods for railway vehicles. Proceedings of the Institution of Mechanical Engineers Part F Journal of Rail and Rapid Transit. 2007; 217(2), 73-88.

[16] Garg V. K. Dynamics of Railway Vehicle Systems. New York: Academic Press. 1984.

[17] Mansfield N J. Literature review on low frequency vibration comfort. Report under EU Asia Link Program. 2005; 109.

[18] Hughes H, Gleason, McCallum et al. Calculus, third edition. John Wiley & Sons, Inc. 2002.

Appendix

The equations of motion for the first wheelset, first bogie frame, and car body are written as:

$$\begin{cases} m_w\ddot{y}_{w1}+(2c_{py}+2f_{22}/v)\dot{y}_{w1}+2k_{py}y_{w1}+2c_{py}(h_{psf}\dot{\varphi}_{f1}-\dot{y}_{f1}-h_{da}\dot{\psi}_{f1})+2k_{py}(h_{psf}\varphi_{f1}-y_{f1}-h_{da}\psi_{f1})-2f_{22}\psi_{w1}=0 \\ I_{wz}\ddot{\psi}_{w1}-(k_{\varphi}-2k_{px}h_{dp}^{\ 2})\psi_{w1}+(2f_{11}s^2/v+2c_{px}h_{dp}^{\ 2})\dot{\psi}_{w1}-2c_{px}h_{dp}^{\ 2}\dot{\psi}_{f1}-2k_{px}h_{dp}^{\ 2}\psi_{f1}=0 \end{cases} \tag{A1}$$

$$\begin{cases} m_f\ddot{y}_{f1}+(4c_{py}+2c_{sy})\dot{y}_{f1}+(4k_{py}+2k_{sy})y_{f1}-2c_{py}(\dot{y}_{w1}+\dot{y}_{w2}+2h_{psf}\dot{\varphi}_{f1})-2k_{py}(y_{w1}+y_{w2}+2h_{psf}\varphi_{f1}) \\ \quad +2c_{sy}((h_{ssc}-h_{df})\dot{\psi}_c+h_{ssf}\dot{\varphi}_{f1}-\dot{y}_c)+2k_{sy}((h_{ssc}-h_{df})\psi_c+h_{ssf}\varphi_{f1}-y_c)=0 \\ m_f\ddot{z}_{f1}+(4c_{pz}+2c_{sz})\dot{z}_{f1}+(4k_{pz}+2k_{sz})z_{f1}+2c_{sz}(h_{df}\dot{\theta}_c-\dot{z}_c)+2k_{sz}(h_{df}\dot{\theta}_c-z_c) \\ \quad +2c_{pz}(\dot{z}_{w1}+\dot{z}_{w2})+2k_{pz}(z_{w1}+z_{w2})=0 \\ I_{fx}\ddot{\varphi}_{f1}+(4c_{pz}h_{dp}^{\ 2}+2c_{sz}h_{ds}^{\ 2}+4c_{py}h_{psf}^{\ 2}+2c_{sy}h_{ssf}^{\ 2})\dot{\varphi}_{f1}+(4k_{pz}h_{dp}^{\ 2}+2k_{sz}h_{ds}^{\ 2}+4k_{py}h_{psf}^{\ 2}+2k_{sy}h_{ssf}^{\ 2})\varphi_{f1} \\ \quad -(2k_{sz}h_{ds}^{\ 2}-2k_{sy}h_{ssc}^{\ 2})\varphi_c-(2c_{sz}h_ds^2-2c_{sy}h_{ssc}^{\ 2})\dot{\varphi}_c-(4c_{py}h_{psf}-2c_{sy}h_{ssf})\dot{y}_{f1}-(4k_{py}h_{psf}-2k_{sy}h_{ssf})y_{f1} \\ \quad +2c_{py}h_{psf}(\dot{y}_{w1}+\dot{y}_{w2})-2c_{sy}h_{ssf}\dot{y}_c-2k_{sy}h_{ssf}y_c+2k_{py}h_{psf}(y_{w1}+y_{w2})-2c_{sy}h_{df}h_{ssf}\dot{\psi}_c-2k_{sy}h_{df}h_{ssf}\psi_c=0 \\ I_{fy}\ddot{\theta}_{f1}+(4c_{pz}h_{da}^{\ 2}+4c_{px}h_{psf}^{\ 2}+2c_{sx}h_{ssf}^{\ 2})\dot{\theta}_{f1}+(4k_{pz}h_{da}^{\ 2}+4k_{px}h_{psf}^{\ 2}+2k_{sx}h_{ssf}^{\ 2})\theta_{f1}+2c_{sx}h_{ssc}^{\ 2}\dot{\theta}_c+2k_{sx}h_{ssc}^{\ 2}\theta_c \\ \quad -2c_{pz}h_{da}(\dot{z}_{w1}-\dot{z}_{w2})+2k_{pz}h_{da}(z_{w1}-z_{w2})=0 \\ I_{fz}\ddot{\psi}_{f1}+(4c_{py}h_{da}^{\ 2}+4c_{px}h_{dp}^{\ 2}+2c_{sx}h_{ds}^{\ 2})\dot{\psi}_{f1}+(4k_{py}h_{da}^{\ 2}+4k_{px}h_{dp}^{\ 2}+2k_{sx}h_{ds}^{\ 2})\psi_{f1}-2c_{py}h_{da}(\dot{y}_{w1}-\dot{y}_{w2}) \\ \quad -2k_{py}h_{da}(y_{w1}-y_{w2})-2c_{px}h_{dp}^{\ 2}(\dot{\psi}_{w1}+\dot{\psi}_{w2})-2k_{px}h_{dp}^{\ 2}(\psi_{w1}+\psi_{w2})-2c_{sx}h_{ds}^{\ 2}\dot{\psi}_c-2k_{sx}h_{ds}^{\ 2}\psi_c=0 \end{cases} \tag{A2}$$

$$\begin{cases} m_c\ddot{y}_c+2c_{sy}(2\dot{y}_c-\dot{y}_{f1}-\dot{y}_{f2})+2k_{sy}(2y_c-y_{f1}-y_{f2}) \\ \quad -2c_{sy}(2h_{ssc}\dot{\varphi}_c+h_{ssf}\dot{\varphi}_{f1}+h_{ssf}\dot{\varphi}_{f2})-2k_{sy}(2h_{ssc}\varphi_c+h_{ssf}\varphi_{f1}+h_{ssf}\varphi_{f2})=0 \\ m_c\ddot{z}_c+2c_{sz}(2\dot{z}_c-\dot{z}_{f1}-\dot{z}_{f2})+2k_{sz}(2z_c-z_{f1}-z_{f2})=0 \\ I_{cx}\ddot{\varphi}_c+(2c_{sz}h_{ds}^{\ 2}+2c_{sy}h_{ssc}^{\ 2})2\dot{\varphi}_c+(4k_{sz}hds^2+4k_{sy}h_{ssc}^{\ 2})\varphi_c-(2c_{sz}h_{ds}^{\ 2}-2c_{sy}h_{ssc}h_{ssf})(\dot{\varphi}_{f1}+\dot{\varphi}_{f2}) \\ \quad -(2k_{sz}h_{ds}^{\ 2}-2k_{sy}h_{ssc}h_{ssf})(\varphi_{f1}+\varphi_{f2})-2c_{sy}h_{ssc}(2\dot{y}_c-\dot{y}_{f1}-\dot{y}_{f2})-2k_{sy}h_{ssc}(2y_c-y_{f1}-y_{f2})=0 \\ I_{cy}\ddot{\theta}_c+(4c_{sz}h_{df}^{\ 2}+4c_{sx}h_{ssc}^{\ 2})\dot{\theta}_c+(4k_{sz}h_{df}^{\ 2}+4k_{sx}h_{ssc}^{\ 2})\theta_c+2c_{sz}h_{df}(\dot{z}_{f1}-\dot{z}_{f2})+2k_{sz}h_{df}(z_{f1}-z_{f2}) \\ \quad +2c_{sx}h_{ssf}h_{ssc}(\dot{\theta}_{f1}+\dot{\theta}_{f2})+2k_{sx}h_{ssf}h_{ssc}(\theta_{f1}+\theta_{f2})=0 \\ I_{cz}\ddot{\psi}_c+(4c_{sy}h_{df}^{\ 2}+4c_{sx}h_{ds}^{\ 2})\dot{\psi}_c+(4k_{sy}h_{df}^{\ 2}+4k_{sx}h_{ds}^{\ 2})\psi_c+2c_{sy}h_{df}(\dot{y}_{f1}-\dot{y}_{f2})+2k_{sy}h_{df}(y_{f1}-y_{f2}) \\ \quad -2c_{sx}h_{ds}^{\ 2}(\dot{\psi}_{f1}+\dot{\psi}_{f2})-2c_{sy}h_{df}h_{ssf}(\dot{\varphi}_{f1}-\dot{\varphi}_{f2})-2k_{sx}h_{ds}^{\ 2}(\psi_{f1}+\psi_{f2})-2k_{sy}h_{df}h_{ssf}(\varphi_{f1}-\varphi_{f2})=0 \end{cases} \tag{A3}$$

where, y_w, z_w, ψ_w, y_f, z_f, φ_f, θ_f, ψ_f, y_c, z_c, φ_c, θ_c and ψ_c represent wheel-axle set lateral displacement, vertical displacement and yaw displacement, truck frame lateral displacement, vertical displacement, roll displacement, pitch displacement and yaw displacement, and car body lateral displacement, vertical displacement, roll displacement, pitch displacement and yaw displacement, respectively. Other parameters and corresponding numerical values are shown in Tab. A1.

Tab.A1 Parameter list

Symbol	Variable name	Value	Unit
m_b	Mass of car body	40×10^3	kg
I_{bx}	Longitudinal moment of inertia of car body	120×10^3	kg·m^2
I_{by}	Lateral moment of inertia of car body	1700×10^3	kg·m^2
I_{bz}	Vertical moment of inertia of car body	1600×10^3	kg·m^2
m_f	Mass of bogie	2.6×10^3	kg
I_{fx}	Longitudinal moment of inertia of bogie	1.8×10^3	kg·m^2
I_{fy}	Lateral moment of inertia of bogie	1.1×10^3	kg·m^2
I_{fz}	Vertical moment of inertia of bogie	2.8×10^3	kg·m^2
m_w	Mass of wheelset	1.7×10^3	kg
I_{wx}	Longitudinal moment of inertia of wheelset	0.7×10^3	kg·m^2
I_{wy}	Lateral moment of inertia of wheelset	0.1×10^3	kg·m^2
I_{wz}	Vertical moment of inertia of wheelset	0.7×10^3	kg·m^2
k_{sz}	Vertical stiffness of secondary suspensions	0.6×10^3	kN/m
k_{pz}	Vertical stiffness of primary suspensions	1.3×10^3	kN/m
c_{sz}	Vertical damping of secondary suspensions	15	kN·s/m
c_{pz}	Vertical damping of primary suspensions	15	kN·s/m
k_{sy}	Lateral stiffness of secondary suspensions	0.5×10^3	kN/m
k_{py}	Lateral stiffness of primary suspensions	6.4×10^3	kN/m
c_{sy}	Lateral damping of secondary suspensions	15	kN·s/m
c_{py}	Lateral damping of primary suspensions	0	kN·s/m
k_{sx}	Longitudinal stiffness of secondary suspensions	0.5×10^3	kN/m
k_{px}	Longitudinal stiffness of primary suspensions	14×10^3	kN/m
c_{sx}	Longitudinal damping of secondary suspensions	40	kN·s/m
c_{px}	Longitudinal damping of primary suspensions	0	kN·s/m